The 21st International Conference on
Thermal Science and Engineering of Serbia
SimTerm 2024
Niš, Serbia, Oct 22-25 2024
doi: 10.5937/SimTerm24403S

In-Depth Examination of Water Jet Formations and Patterns at Dam Outlets: Comparative Investigation Employing CFD Simulations and On-Site Drone Footage

Filip Stojkovski[a], Robert Broz[b], Sašo Belšak[c], Valentino Stojkovski[d]

[a] *Iskra Impuls Kranj, Engineering Division Maribor, Maribor, SI, filip.stojkovski@iskraimpuls.si*
[b] *Iskra Impuls Kranj, Engineering Division Maribor, Maribor, SI, robert.broz@iskraimpuls.si*
[c] *Iskra Impuls Kranj, Engineering Division Maribor, Maribor, SI, saso.belsak@iskraimpuls.si*
[d] *"Ss. Cyril and Methodius" University in Skopje, Faculty of Mechanical Engineering Skopje, MK, valentino.stojkovski@mf.edu.mk*

Abstract: This scientific paper presents a comprehensive study on the Computational Fluid Dynamics (CFD) modeling of water jet formations at dam bottom outlets, with a focus in the comparative analysis of CFD results against actual drone footage captured on-site. The research commences with the development of a detailed CFD models, encompassing the geometric and hydraulic characteristics of the dam bottom outlet structure. Special attention is given to incorporating boundary conditions and numerical schemes that accurately simulate the water jet formation process. Computational simulations are conducted for a range of operational scenarios i.e. bottom outlet gate openings. To validate the CFD results and prove their applicability, a field campaign is carried out, involving the use of camera equipped drone and one stationary camera, to capture real-time footage of water jet formations at dam bottom outlet. The drone footage provides invaluable visual data that allows a direct comparison between the CFD predictions and actual on-site observations. The comparative analysis involves a quantitative assessment of key parameters, such as jet velocities, trajectories, flow patterns etc. Discrepancies between the CFD predictions and real-world observations are analyzed to identify potential areas for model refinement and future improvement. The results of this research contribute to a better understanding of the hydraulic behavior of dam bottom outlets. By leveraging advanced CFD modeling and real-world drone footage, this study provides a holistic approach to studying water jet formations at dam outlets, bridging the gap between numerical simulations and empirical observations in a complex hydraulic environment.

Keywords: Computational Fluid Dynamics (CFD), Water Jet Formations, Comparative Analysis, Dam Bottom Outlet, Hydraulic Modeling, Volume of Fluid (VOF), Multiphase Flow.

1. Introduction

Dams are vital infrastructural components that serve a multiple purposes, such as water supply, flood control, irrigation and hydroelectric power generation. Ensuring the safe and efficient operation of dams is of paramount importance, as their failure can have catastrophic consequences. One critical aspect of dam operation is the controlled release of water through bottom outlet, a process that involves the formation of high-velocity and long-spanned water jets. These jets are responsible for discharging water from the reservoir and can exert considerable forces on the outlet hydraulic steel structure.

Traditional engineering approaches have relied on empirical correlations and simplified analytical models to estimate jet characteristics and discharge ratios. While these methods have been valuable in practice, they often lack the precision needed to account for the complex flow phenomena that occur in dam bottom outlets, such as spraying, water-air mixtures etc. A certain time ago model tests were also conducted for this type of hydraulic infrastructures, but today they are more and more abandoned, as the prices for doing such a laboratory (scaled model) research are very high.

Recent advancements in Computational Fluid Dynamics (CFD) have provided engineers and researchers with powerful tools to simulate and analyze fluid flow and its complex flow phenomena. CFD offers the capability to model the fluid flow behavior with a high degree of fidelity, making it an ideal choice for studying the flow patterns associated with water jet formations in dam outlets. However, the successful application of CFD in this context requires rigorous validation against real-world observations, which is the primary objective of this paper.

The motivation for this research arises from the need to bridge the gap between theoretical simulations and practical field data. By combining state-of-the-art CFD modeling with actual drone footage captured at dam

site, we aim to enhance our understanding of water jet formations and validate the accuracy of numerical predictions. Such validation is critical for the broader adoption of CFD in dam engineering and the development of reliable guidelines for outlets design, maintenance and safety.

This paper is structured to provide a comprehensive investigation into the hydraulic behavior of dam bottom outlets, with a specific focus on water jet formations. In addition to the abstract's outlined methodology, the subsequent sections will delve into the details of the CFD model setup, field data acquisition, and the comparative analysis of results. The findings of this study will not only contribute to the scientific understanding of water jet formations, but also serve as a practical resource for hydro engineers seeking to improve their understandings of the subject, for future hydro-mechanical equipment development.

2. Case Study Description

Dams and hydropower facilities in the Balkan region, particularly in the former Yugoslavian countries, are approaching a phase where the consideration of reconstruction is imperative. This is done with the aim of extending their operational lifespan and enhancing their performance. Specifically, the reconstruction of hydraulic gates on the dam bottom outlets is a task that lacks standardized guidelines and is primarily reliant on the practical experience accumulated by engineers over the years of working with such equipment. To assess the scope of refurbishment required for a hydraulic gate, it is essential to undertake analytical and numerical calculations, to anticipate on-site conditions, expected loads, hydrodynamic forces, discharge rates and outflow conditions and other relevant factors [11, 12].

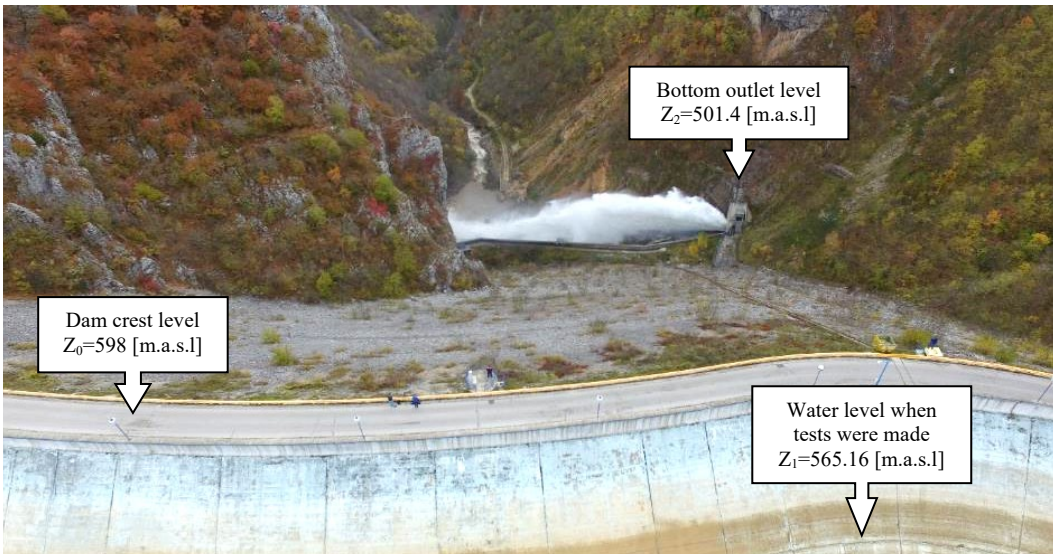

Figure 1. View on the dam crest and bottom outlet configuration.

Back in the 60's, a fixed-wheel vertical bonneted gate was installed at the outlet section of the dams' bottom outlet tunnel. The gate's dimensions, including gate body height, span and depth are 4.3x3.3x0.75 [m], respectively. The gate lip at the lower seal is profiled and has a 45 [°] slope angle. To operate the gate, a hydraulic cylinder is mounted on the top of the gate casing cover, connected directly without the use of lifting rods. The gate can be lifted to a maximum height of 4.2 [m], while the net clearance height for the bottom outlet is Z_0=4 [m], creating a net cross-sectional area of 4x1.9 [m] i.e. A_0=7.6 [m^2]. The bottom outlet has an inclination slope of approximately +8 [°], resulting in an outflow resembling projectile motion in the form of a jet. The concrete channel where the jet is formed is with side slopes of +7 [°], which start immediately after the gate body [11].

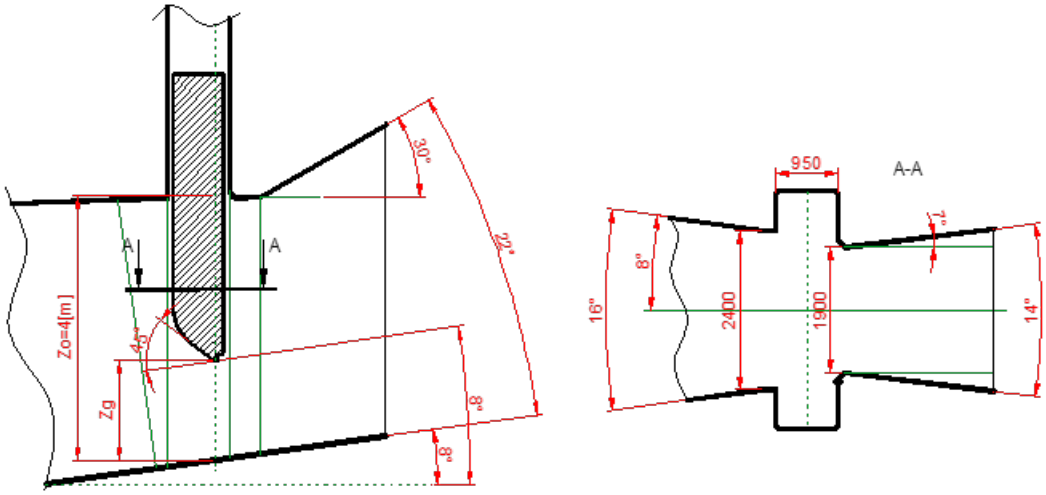

Figure 2. Bottom outlet gate section dimensions.

The outlet terrain slope was taken from the geodetic measurements available. Having that data, primarily a theoretical calculations were made to see the expected jet length and size. Using the simple kinematic theory of projectile motion, the water was taken as massless object without air resistance. For the given conditions, the following model was used:

$$y = \mathrm{x} \cdot \tan\theta - \frac{\mathrm{g} \cdot \mathrm{x}^2}{2 \cdot \mathrm{v}_0^2} \cdot (1 + \tan^2\theta) \tag{1}$$

where x is the terrain length coordinates, v_0 is the water velocity under the gate, θ is the angle of the bottom outlet inclination slope and g is the gravitational acceleration. The theoretical velocity under the gate is calculated according the Torricelli formula as [1, 2]:

$$\mathrm{v}_0 = \sqrt{2 \cdot \mathrm{g} \cdot \left(\mathrm{H} - \mathrm{C}_\mathrm{c} \cdot \mathrm{Z}_\mathrm{g}\right)} \tag{2}$$

where H is the water column in the reservoir, $\mathrm{C_c}$ is the contraction coefficient of the gate lip, where acc. to [1] for 45 [°] gate lip $\mathrm{C_c} \approx 0.75$, and $\mathrm{Z_g}$ is the gate opening height. From this relations, the following chart was obtained. Having these conditions in-mind, the computational domain was created, using the terrain data, but simplified, and the length of the theoretical jet.

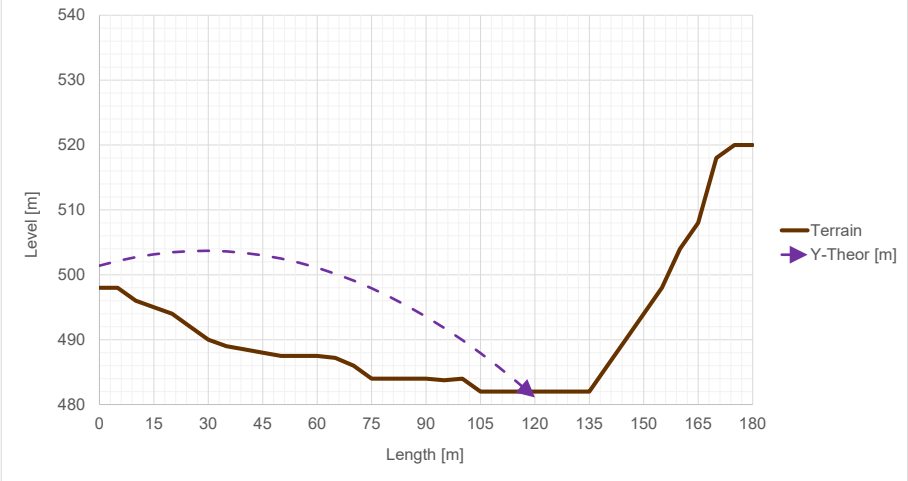

Figure 3. Terrain configuration and theoretical jet length calculated for gate opening of 50 [%].

3. Numerical Modeling

Numerical simulations were conducted using a true-scale model of the dam's bottom outlet. The simulations were carried out using the Ansys Fluent software. To accurately capture the narrow spaces between the gate and the bonnet, a Watertight meshing technique with Polyhedral mesh was employed when creating the

numerical mesh in Fluent Mesher. The outflow region was modeled to replicate the actual on-site conditions. Additionally, a partial representation of the steel liner in the bottom outlet was included in the model to reduce the size of the numerical domain.

3.1. Multiphase Flow Modeling Approach

In order to analyze the water jets formations behind the gate, it is necessary to employ multiphase flow modeling, as the flow in this region is characterized by the creation and dispersion of water jets into the surrounding air [9]. In multiphase flow, a "phase" is defined as a distinct category of material with specific characteristics in response to the flow and the potential field in which it exists. In this context, two phases were considered: air and water. Multiphase flow refers to the simultaneous flow of multiple phases, making it a two-phase flow scenario.

Because the two phases are interpenetrating between each other, the Euler-Euler Volume of Fluid (VOF) approach in multiphase modeling was used. This approach involves tracking the interface between two immiscible fluids, such as water and ambient air, on a fixed Eulerian mesh. In the VOF model, a single set of momentum equations is shared by both fluids, and the volume fraction of each fluid in each computational cell is continuously tracked throughout the domain. This methodology is well-suited for predicting phenomena like jet breakup, liquid motion after a dam break, free surface flows and tracking of liquid-gas interfaces, whether in steady or transient scenarios [4].

The VOF formulation is based on the principle that multiple fluids do not mix with each other [4]. When introducing an additional phase into the model, a new variable is introduced, which represents the volume fraction of that phase within each computational cell. These variables and properties are shared among all the phases and represent volume-averaged values, provided that the volume fraction of each phase is known at every location. Consequently, the variables and properties within a cell can either exclusively represent one of the phases or represent a combination of the phases, depending on the volume fraction values. To track the interface between the phases, a continuity equation for the volume fraction of one of the phases is solved:

$$\frac{1}{\rho_q}\left[\frac{\partial}{\partial t}\left(\alpha_q\rho_q\right) + \nabla\cdot\left(\alpha_q\rho_q\overrightarrow{v_q}\right) = S_{\alpha_q} + \sum_{p=1}^{n}\left(\dot{m}_{pq} - \dot{m}_{qp}\right)\right] \tag{3}$$

where $\dot{m}_{qp}$ is the mass transfer from phase q to phase p, and $\dot{m}_{pq}$ denotes the reverse transfer. In this specific scenario, right-hand side of this equation is not relevant because there is no mass transfer mechanism present. So, the volume fraction inside a cell of the mesh is computed for the secondary phase (the driving phase - water) starting as:

$$\sum_{q=1}^{n}\alpha_q = 1 \tag{4}$$

When α_q falls within the range of 0 to 1, it signifies the presence of an interface between the phases. An implicit scheme was employed to concurrently solve the phase continuity equation alongside iterations involving momentum and pressure. In a two-phase system designated as phases 1 and 2, where the second phase serves as the driving phase, the density and viscosity in each cell were computed as follows:

$$\rho = \alpha_2\rho_2 + (1-\alpha_2)\rho_1\ ;\ \mu = \alpha_2\mu_2 + (1-\alpha_2)\mu_1 \tag{5}$$

The calculation method for all other physical properties remains consistent. A unified momentum equation is resolved across the entire domain, and the resultant velocity field is applied to all the phases. The expressions for the continuity and momentum equations governing the mixture of phases are as follows:

$$\begin{gathered}\frac{\partial}{\partial t}(\rho\vec{v}) + \nabla\cdot(\rho\vec{v}) = S \\ \frac{\partial}{\partial t}(\rho\vec{v}) + \nabla\cdot(\rho\vec{v}\vec{v}) = -\nabla p + \nabla\cdot\left[\mu\left(\nabla\vec{v} + \nabla\vec{v}^{T}\right)\right] + \rho\vec{g} + \overrightarrow{T_\sigma}\end{gathered} \tag{6}$$

which are dependent from the volume fractions of the phases thorough the density and viscosity from Eq.5. Based on the local value of α_q, the appropriate properties and variables are assigned to each control volume within the domain.

The modeling approach employed for the fractional interface is referred to as "Sharp", specifically between water and air. It is calculated using the "Compressive Interface" capturing scheme, which is well-suited for "Steady-State Implicit" solutions employing the "Implicit Body Force" formulation. In this analysis, the Energy equation was omitted because heat transfer and the physical properties of the surrounding air, such as compressibility, are considered insignificant. Although the surface tension between the phases is exceptionally small, it is present from physical standpoint, and for the modeling purposes, it was set at 0.072 [N/m] as a continuum surface force between air and water.

3.2. Computational Domain and Boundary Conditions

Figure 4 provides an illustration of the computational domain along with its boundary conditions. This domain encompasses several components: a section of the steel liner originating from the bottom outlet, a reducer, the gate body enclosed in the bonnet, the outlet terrain slope, and the surrounding ambient volume. The operating pressure was set to atmospheric pressure of $p_{atm} = 101325$ [Pa], and the gravity was applied vertically with $g_Z = -9.81$ [m/s^2].

At the inlet, the total pressure was defined based on the water level in the reservoir, which corresponds to the water level when the footage was made, i.e $H_W = 63.76$ [m] or $p_{inlet} = 624311$ [Pa]. At the inlet in front of the gate, the secondary (driving) phase was imposed as 100 [%] water presence. The outlet sections are represented with the pressure outlet boundary conditions. On the top of the domain was given a static pressure outlet with 0 [Pa] intensity, with imposed primary phase (air) of 100 [%]. On the left, right and front side of the outlet domain, the pressure outlet boundary condition was imposed, with enabled Open-Channel condition, giving a negligible small free surface water level of 1 [m], to address that it represents an outflow of the secondary phase (water). As it was mentioned, the numerical mesh was developed as Polyhedral mesh. The models is consisted of cca. 600.000 cells.

The chosen turbulence model was Standard *k-ε*. The Coupled solver was enabled, coupled with the Volume Fractions. Additionally, Pseudo-Transient mode was initiated to adress the Navier-Stokes equations. Even though the simulations were set-up as Steady State, the Pseudo-Transient mode introduces a "fictional" time step to enhance convergence when dealing with volume fractions between phases. The ultimate outcome of the case still represents a Steady-State solution. Convergence of the residuals was achieved, reaching a value of 10^{-5}.

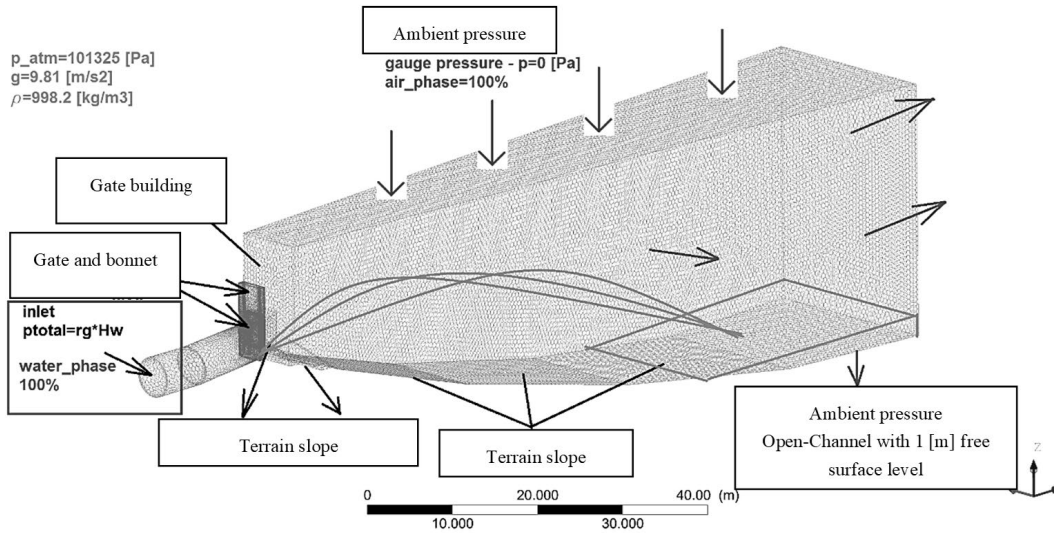

Figure 4. Computational Domain and Boundary Conditions.

4. Simulation Results

In this section, the outcome of the simulations is presented. Previous analysis [11] were conducted to estimate the hydrodynamic forces on the gate, by measuring the lifting pressures and comparing them with the numerical simulations, where matched results were obtained. This was a part of a reconstruction project that our company had to make 2 years ago, in order to develop a quality analysis of the scope of works, loads and all the phenomena occurring on-site, via numerical simulations. Within this chapter, we delve into the analysis

of water jet formations behind the gate and compare them with drone footage captured during on-site tests. Unfortunately, the footage only covers up to 50 [%] of the gate's opening, so our results are limited to this range of gate positions. Based on this comparisons, we found a strong agreement between the CFD results and the footage.

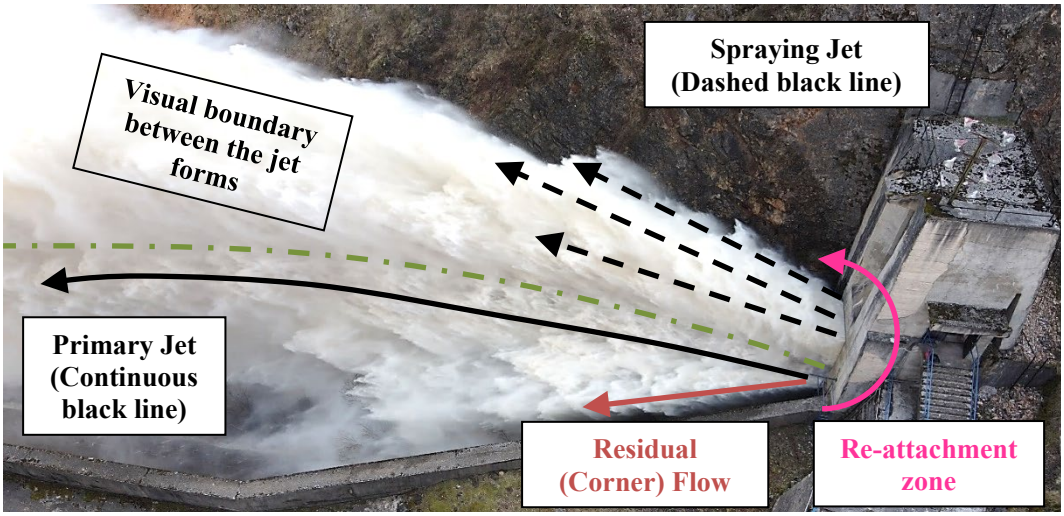

Figure 5. Description of primary jet and spray jet flow patterns.

Evaluating a pure water jet can be challenging since the actual outflow represents a mixture of water and air phases, characterized by spraying of non-interpenetrating phases, shown as water dispersion into the surrounding environment. As the gate opens, high pressure of water is converted into a flow, in a form of a water jet. The water flow profile "expands" in the opened chamber just behind the gate, forming two visual jet configurations: Primary jet (this pattern is in the lower zone) and Spraying jet (expanded flow pattern mixed with air, attached on the ceiling of the chamber – upper zone).

From the video footages it can be seen that the primary jet flow pattern has higher velocity than the spraying jet, and it is representing the simplified kinematic pattern of water flow. The spraying jet is formed in a complex manner. The expanded water which attaches on the top of the chamber ceiling, firstly it slows down, than it recirculates. One part of it, travels forward with decreased velocity at the beginning, reattaches on the primary jet and then travel together. The other detaches from the ceiling, recirculates and sticks on the primary jet, forming a top corner flow pattern, and they travel together too. These phenomena were detected in several simulations which are described further in this chapter.

The following figures depicts sequential snapshots of the gate opening from 0 to 50 [%] offering a comparison with drone footage images taken under identical operating conditions. Overlapping of the simulation results and the actual footage was made to see the jet formation and following phenomena which occur.

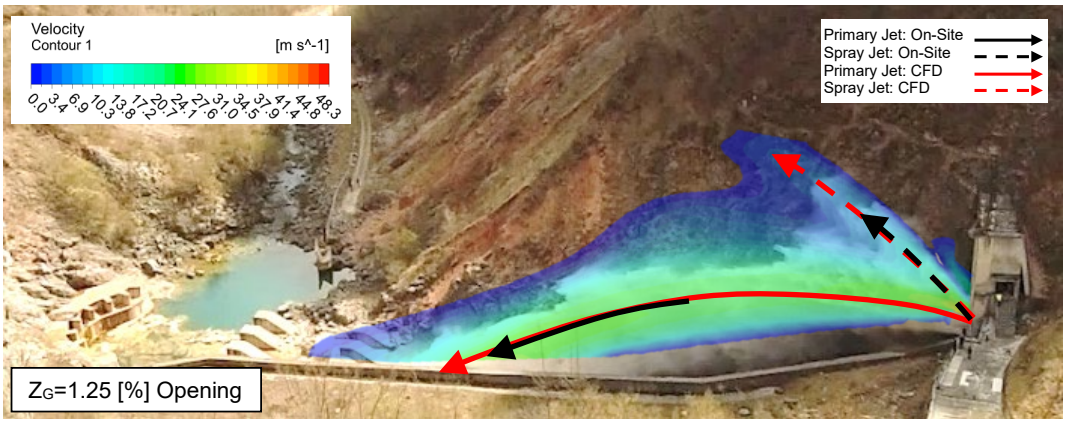

Figure 6. Gate opening at 1.25 [%] – Start.

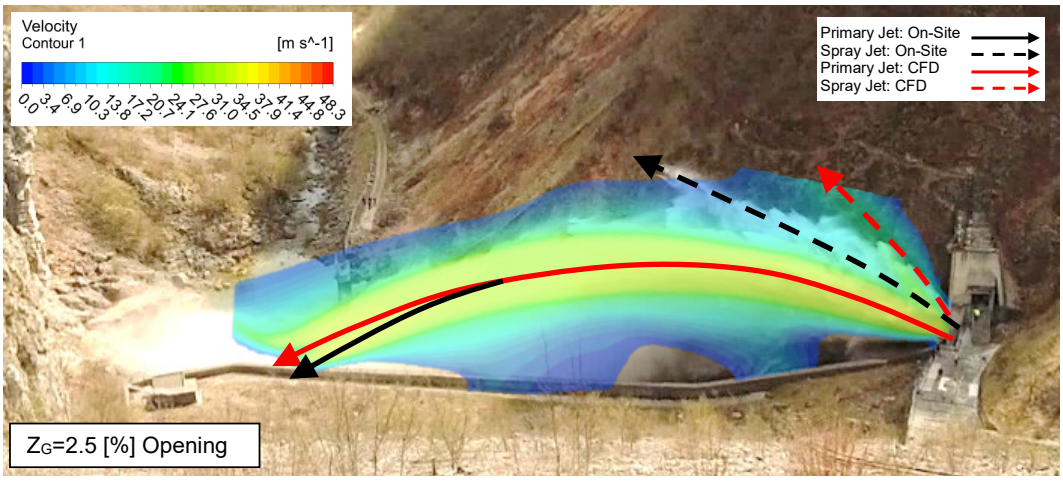

Figure 7. Gate opening at 2.5 [%].

Figures 6 and 7 reveal that, under these specific partial operating conditions, the water jet formations obtained through CFD align closely with the real-world on-site conditions. On figure 7 for gate opening of 1.25 [%] it can be seen the two characteristic flow patterns described earlier. The computed primary jet and the spraying jet perfectly matches the on-site conditions. Compared with the flow on figure 7 for 2.5 [%] a slight discrepancy is obtained in the spraying jet pattern between the on-site and numerically obtained results. The discrepancies between those two is considered to originate from the "tightness" of the modeled computational domain, especially by height, to capture the spraying patterns more precisely. The computed primary jet pattern overlaps perfectly with the on-site conditions, by length and by its "parabola" height.

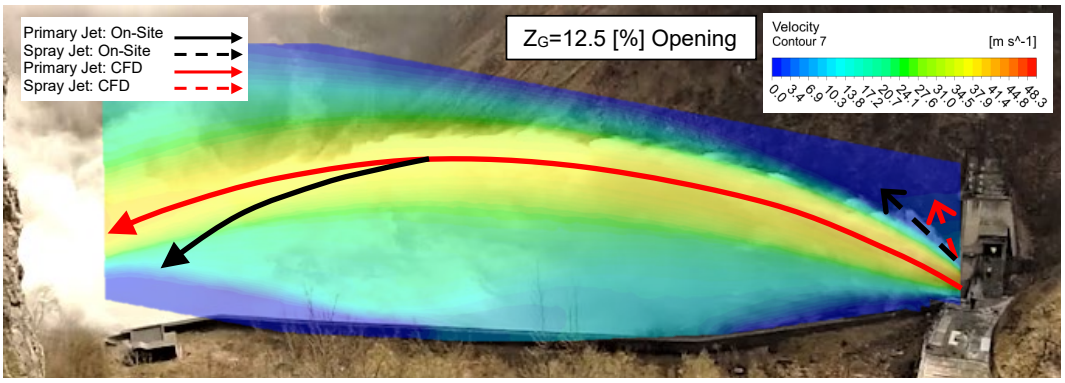

Figure 8. Gate opening at 12.5 [%].

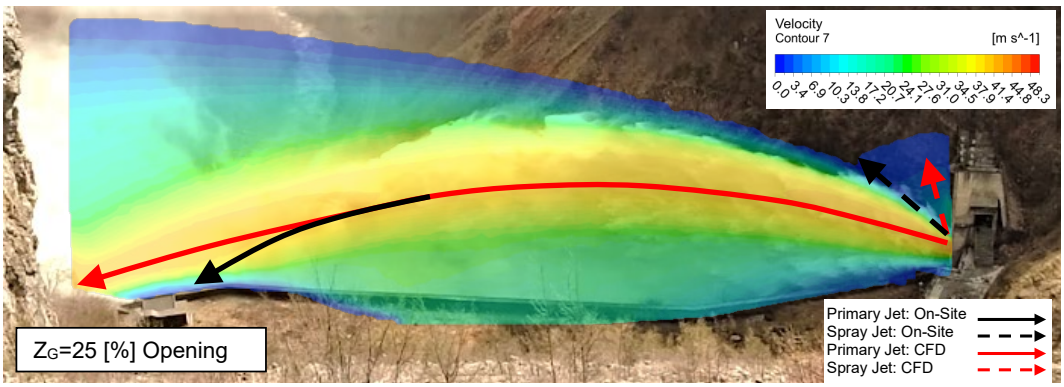

Figure 9. Gate opening at 25 [%].

On figure 8 for gate opening of 12.5 [%], it can be seen that the spray jet is present on-site with decreased intensity, and also in the computed results, which shows a good prediction, with slight discrepancy in the slope. One discrepancy is obtained between the computed results and the on-site conditions, in the primary jet length. Same as the previous scenario, here on figure 9 it can be seen similar discrepancies for 25 [%] of gate opening.

On figure 10 for gate opening of 50 [%], it can be seen that the length discrepancy of the computed primary jet with the actual on-site footage is shortened, which shows that the overall jet behavior and form is highly dependent from the gate opening. For smaller openings than 50 [%], the water jet is characterized with increased height and length, but without any intensity, as the gate interferes the flow substantially. When the gate is opened at 50 [%], the jet is more "firm", almost fully formed and it is characterized by almost fixed length and height, with less other phenomena occurring, like sprays and etc.

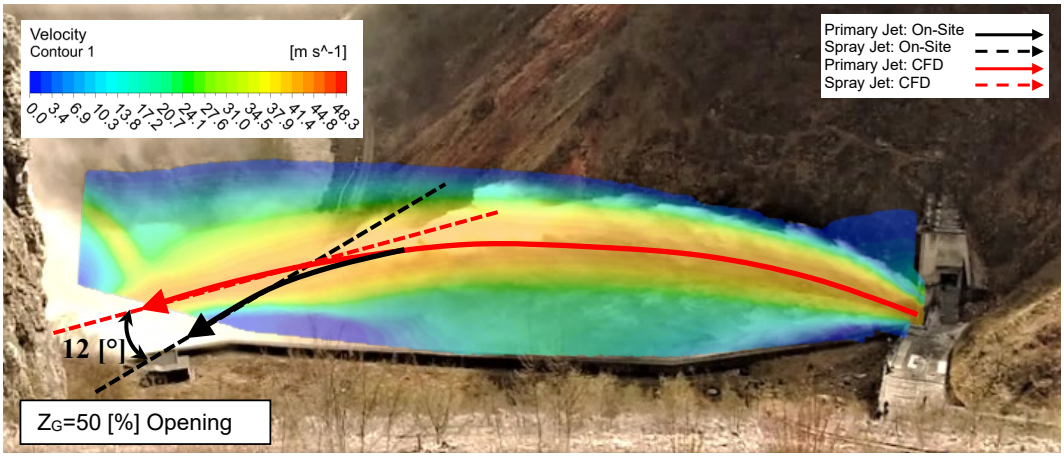

Figure 10. Gate opening at 50 [%].

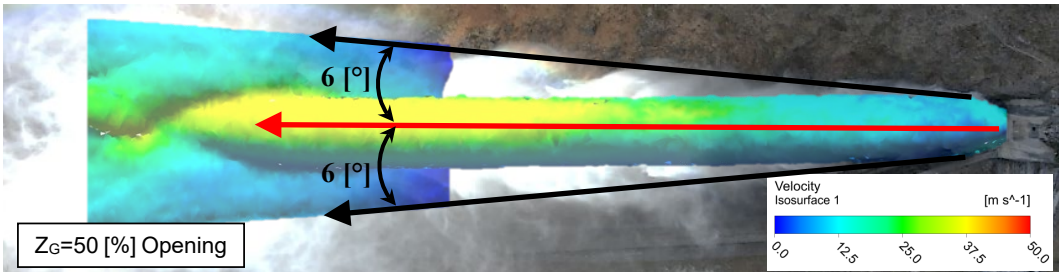

Figure 11. Gate opening at 50 [%] – Top view.

Other discrepancy noticed is shown on figure 11 where the top view shows the on-site jet expands, and the computed one is rather straight. By measuring the tangency of the angles where the primary jet is on-site shortened than the calculated one, we can see a discrepancy of cca. 12 [°]. On the top view, measuring the discrepancies in the jet spreading, we can see a discrepancy of cca. 2 x 6 [°] = 12 [°], which is same as the length shortening angle. This indicates that the jet spreading in real-world conditions results in jet shortening by length. Possible solution to outcome this situation can be in the geometric modeling of the computational domain, which shows that increasing the width of the domain might lead to jet spreading.

On figure 13 the jet cross sections are shown. As the surface under the gate is rectangular, when it's opened, on-site cross sections of the jet are expected to be similar to rectangular shape, shown in figure 12. The simulated jet has rounded circular shape. Possible solution to outcome this situation can be in the boundary conditions applied on the sides of the domain, which are adopted as pressure boundaries. Perhaps symmetry or wall boundary conditions would lead to a better prediction of the jet cross section, jet spread, and with that, the jet length.

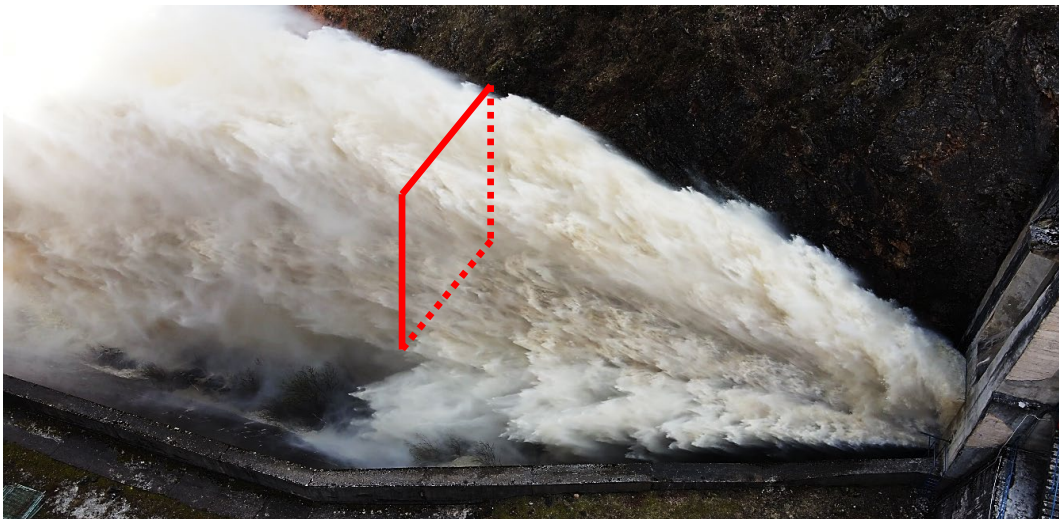

Figure 12. Visual on-site jet cross section.

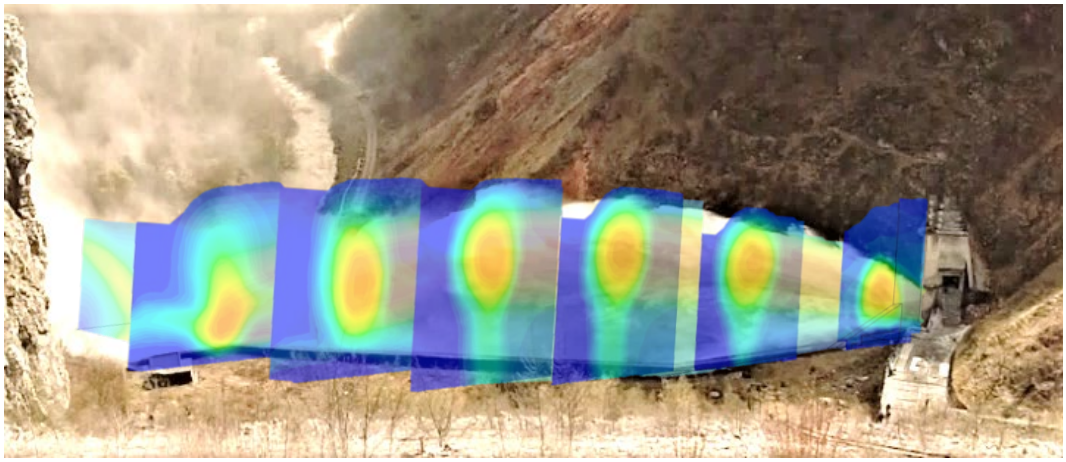

Figure 13. Jet cross section profiles for gate opening of 50 [%].

As it is shown, the on-site conditions shows that the jet spreads and shrinks, compared with the CFD results, an orthogonal projection of the CFD results was made and plotted against the theoretical calculated jet length. It can be seen on the chart on figure 14 that the CFD calculated jet length is shorter and milder than the theoretical jet assumed as pure projectile movement, for cca. 25-30 [m] difference. This shows that despite of the discrepancies obtained from the numerical simulations, still the CFD solution is far closer to the on-site flow conditions than the theoretical approach.

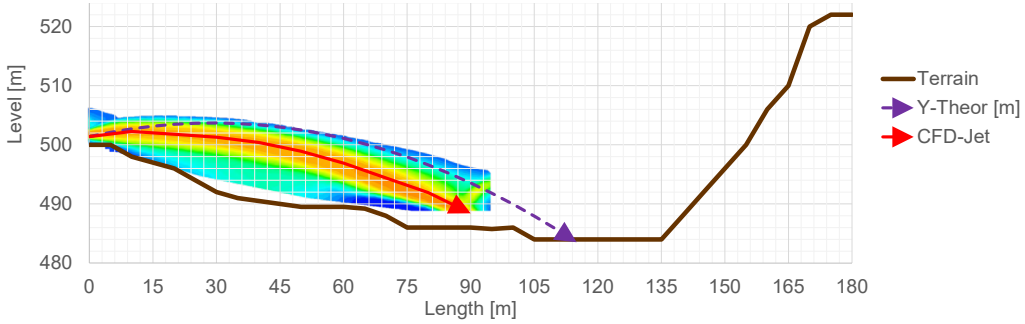

Figure 14. Comparison between CFD results and theoretical jet length for 50 [%] gate opening.

One step further was made to ensure that the results are in good correspondence with the on-site conditions, with comparing the discharge rates from the CFD analysis with an available old data from model tests for the bottom outlet. The results show good overlapping and satisfactory precision, shown on figure 15. The calculated jet forms and patterns shows that they do not influence on the discharge rate as a parameter, for the given conditions, and also on the hydrodynamic forces on the gate, as previously measured [11].

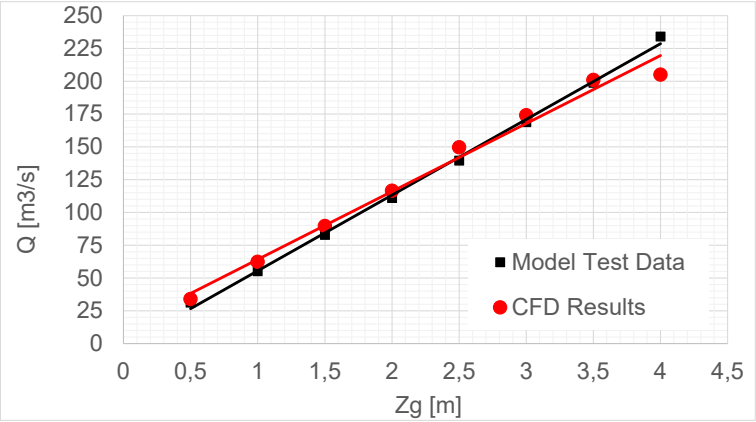

Figure 15. Compared discharge rates with available data from old Model Tests.

5. Conclusions

In this paper, a comprehensive study was carried out on the modelling approach of jet formations at dam bottom outlets, and comparisons of the obtained results with on-site footages. Primarily, the case study was explained, by defining the geometric parameters of the bottom outlet gate and channel, with the terrain slopes and configuration and the estimated theoretical jet length, on which basis the computational domain can be developed.

Second, the numerical approach was defined, by developing a multiphase volume of fluid methodology to capture the wanted effects. By defining the computational domain, the boundary conditions were explained and the solver used to obtain the needed results.

The simulated scenarios are compared with on-site drone footages to see similarities and the discrepancies between the real-world jet formation conditions, and the CFD results. For partial gate openings below 10 [%], the computed results show great match with real-world conditions on-site, by comparing the main outflow jet by length and height, and by comparing the following phenomena which occur, such as the jet sprays. For gate opening from 10 to 25 [%], jet spraying phenomena doesn't occur on-site, and so on the computed results. The main discrepancies here are in the jet length.

For gate opening of 50 [%] which is the maximal opening captured with footages, it can be seen that the computed trajectory of the main jet follows the on-site formed jet, with a discrepancy in the length. Approximately, the angle between the tangencies of the jet length was measured cca. 12 [°]. The top view of the jet shows that real-world jet spreads for about 2 x 6 [°] = 12 [°] compared with the computed one, which indicates that the jet spreading leads to jet shortening. This shows that some model improvements can be made to overcome this discrepancies and to get closer to the on-site conditions. Another comparison was made for the CFD results and the theoretical jet length, where it is shown that the CFD results give closer prediction of the jet length than the theoretical one, plus several jet phenomena were captured like sprays etc. which analytically cannot be obtained.

The discharge rates obtained with the CFD analysis were compared with old model test data of the bottom outlet, where good precision was obtained, showing that despite of the jet form discrepancies, the results are precise.

In summary, this study has provided valuable insights into the modeling of jet formations at dam bottom outlets, highlighting areas of alignment with on-site conditions and opportunities for model enhancements. These findings contribute to our understanding of flow dynamics in such critical engineering structures and offer potential avenues for improved design and performance evaluation in the future.

References

[1] Naudascher E. Hydrodynamic Forces, University of Karlsruhe, Germany, 1991.
[2] Erbisti P.C.F. Design of Hydraulic Gates, 2nd edition. CRC Publishers, 2014.
[3] Fluent 6.3 User's Guide.
[4] Brennen C. Fundamentals of Multiphase Flows. CALTECH, 2005.

[5] Badas M. et al. May a Standard VOF Numerical Simulation Adequately Complete Spillway Laboratory Measurements in an Operational Context? The Case of Sa Stria Dam, Water 2020, 12, 1606; doi:10.3390/w12061606, 2020.
[6] Denner F. Compressive VOF method with skewness correction to capture sharp interfaces on arbitrary meshes, Journal of Physics 279, doi: 10.1016/j.jcp.2014.09.002, pp. 127 – 144, 2014
[7] Hui D. Numerical study of advection schemes for interface-capturing using gradient smoothing method. Numerical Heat Transfer Fundamentals 73(4), doi: 10.1080/10407790.2018.1462005, pp. 242 – 261, 2018.
[8] Viti N. Numerical simulations of Hydraulic Jumps. Part 2: Recent Results and future work. Water 2019, 11, 28; doi:10.3390/w11010028, 2019.
[9] Awad M.M. Two-Phase Flow, doi:10.5772/76201.
[10] Muralha A. Assessment of CFD solvers and turbulent models for Water Free Jets in Spillways, Fluids, 5, 104; doi:10.3390/fluids5030104, 2020.
[11] Stojkovski F. et al., Multiphase Flow Modeling to Predict Hydrodynamic Forces and Outflow Conditions of a Dam Bottom Outlet Regulation Gate. 20th International Symposium of Thermal Engineering, Niš, Serbia, 2022, pp. 361 – 371.
[12] Stojkovski F. et al. Reconstruction Steps to Improve Performance of s Dam Bottom Outlet Regulation Gate. XXXVII International Symposium of Energetics, 21st – 24th June, Zlatibor, Serbia, 2022
[13] Stojkovski F. et al. Challenges in the Design and Construction of a Large Scale Hydro-Mechanical Equipment. XXXVth International Symposium of Energetics, Zlatibor, Serbia, 2020, pp. 305 – 311
[14] DIN19704. Hydraulic Steel Structures, 2004.